

Hybrid Opto-Electrical Excitation of Spin-Transfer Torque Nano-Oscillators for Advanced Computing

Felix Oberbauer^{a,1}, Tristan Joachim Winkel^{a,1}, Tim Böhnert,² Marcel S. Claro,² Luana Benetti,² Ihsan Çaha,² Leonard Francis,² Farshad Moradi,³ Ricardo Ferreira,² Markus Münzenberg,¹ and Tahereh Sadat Parvini^{b4,5,1}

¹*Institut für Physik, Universität Greifswald, 17489 Greifswald, Germany*

²*INL - International Iberian Nanotechnology Laboratory, Avenida Mestre José Veiga, s/n, 4715-330 Braga, Portugal*

³*Electrical and Computer Engineering Department, Aarhus University, 8200 Aarhus, Denmark*

⁴*Walther-Meißner-Institut, Bayerische Akademie der Wissenschaften, 85748 Garching, Germany*

⁵*Munich Center for Quantum Science and Technology (MCQST), Schellingstr. 4, 80799 Munich, Germany*

(Dated: January 3, 2025)

Neuromorphic computing, inspired by the brain’s parallel and energy-efficient information processing, offers a transformative approach for advancing artificial intelligence. In this study, we fabricated optimized spin-transfer torque nano-oscillators (STNOs) as foundational building blocks for neuromorphic systems and investigated their dynamic and functional behaviors using a hybrid excitation scheme that combines AC laser illumination and DC bias currents. Laser-induced thermal gradients across the tunnel barrier generate pulsed thermoelectric voltages (V_{AC}) via the Tunnel Magneto-Seebeck (TMS) effect, while the addition of a bias current results in an enhanced bTMS effect, producing both V_{AC} and a DC component (V_{DC}). Magnetic field sweeps reveal distinct switching between parallel (P) and antiparallel (AP) magnetization states in both V_{AC} and V_{DC} , suggesting potential for multistate memory applications. In open-circuit conditions, the devices exhibit millivolt-range thermovoltage signals, demonstrating direct compatibility with CMOS technology and providing a promising pathway to simplify scalable and energy-efficient neuromorphic

^a These authors contributed equally to this work.

^b Tahereh.Parvini@wmi.badw.de

computing architectures by minimizing wiring complexity. Under biased conditions, the devices generate significantly enhanced thermovoltage outputs and exhibit intriguing phenomena, including thermovoltage spikes and double-switching behavior. The observed spikes are correlated with Barkhausen jumps in the DC output voltage, offering fundamental insights into domain dynamics and vortex-core transitions. Beyond their fundamental importance, these spikes bear a striking resemblance to neural spiking behavior, positioning the system as a promising candidate for applications in spiking neural networks and reservoir computing, where complex nonlinear dynamics and memory effects are critical for efficient information processing. These results position the hybrid system of STNOs and vertical-cavity surface-emitting lasers (VCSELs) as a versatile platform for energy-efficient computing, multistate logic, analog computing, advanced signal processing, high-resolution sensing, and neuromorphic computing applications. By bridging fundamental spintronic phenomena with practical applications, this work lays the foundation for next-generation AI technologies and adaptive computational frameworks.

I. INTRODUCTION

The relentless advancement of artificial intelligence (AI) necessitates revolutionary computing architectures capable of addressing increasingly complex tasks with unprecedented efficiency. Traditional silicon-based systems, rooted in the von Neumann paradigm, are increasingly constrained by critical limitations such as the von Neumann bottleneck, the memory wall, and excessive power consumption [1–3]. These challenges, which are further exacerbated as AI models grow in complexity and data-intensive applications expand, have driven the exploration of alternative paradigms, including quantum [4–8] and neuromorphic computing [9–16]. Neuromorphic computing, inspired by the brain’s parallel and energy-efficient processing capabilities, mimics biological neural networks where artificial neurons and synapses dynamically adjust their states, akin to synaptic plasticity. This paradigm offers a scalable and energy-efficient framework ideally suited for next-generation AI, cognitive computing, and real-time edge processing [17–21].

Spintronic devices [22–24], particularly spin-transfer torque nano-oscillators (STNOs)

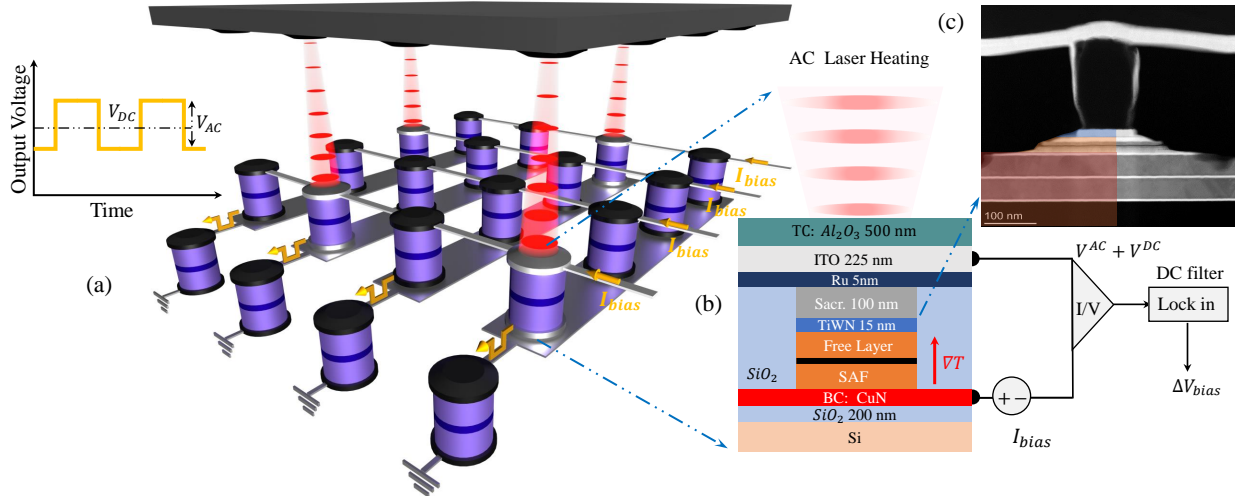


FIG. 1. (a) Schematic representation of a hybrid photonic-spintronic neuromorphic system. The VCSEL array delivers spatially selective optical excitation to an STNO array, enabling independent control and dynamic modulation of individual devices. (b) Configuration of the STNO devices and the fundamental concept underlying the TMS and bTMS experiments. The electrical setup includes a lock-in amplifier, which acts as a filter to isolate the DC signal generated by the bias current. (c) High-Angle Annular Dark-Field Scanning Transmission Electron Microscopy (HAADF-STEM) image of an isolated MTJ nanopillar.

[25–30], have emerged as promising components for neuromorphic computing due to their non-volatility, ultrafast switching capabilities, and energy efficiency. STNOs leverage spin-polarized currents to induce high-frequency oscillations in nanoscale magnetic structures, exhibiting nonlinear dynamics crucial for emulating biological neural networks [31–34]. Vortex-based STNOs offer enhanced stability and robustness through localized magnetic vortex structures, making them suitable for scalable neuromorphic systems [35–38]. While recent progress has demonstrated information encoding through tunable frequency, amplitude, and phase in STNO devices for neuromorphic applications, challenges remain in efficient thermal management, scalable architectures, and developing signal processing techniques that fully exploit their dynamic properties. In this study, we investigate the dynamic behavior of structurally and dimensionally optimized spin-transfer torque nano-oscillators (STNOs) under laser-induced thermal gradients [39–43]. We employ hybrid excitation schemes, combining optical and electrical inputs to enhance functionality and control in STNOs. A modulated diode laser (1 kHz on-off frequency) induces periodic thermal gradients across the tunnel

barrier, generating a pulsed thermoelectric voltage (V_{AC}) via the Tunnel Magneto-Seebeck (TMS) effect, driven by temperature-dependent asymmetry in electronic states. When a bias current is applied, an additional DC voltage (V_{DC}) arises as the baseline of the output pulse. These components are separated and investigated under sweeping magnetic fields to explore their distinct contributions.

The overarching vision of this work is captured in Fig. 1(a), which illustrates a neuromorphic chip integrating spintronic devices with the optical precision of vertical-cavity surface-emitting lasers (VCSELs) for localized excitation. This architecture utilizes programmable VCSEL arrays to selectively activate STNOs, each exhibiting unique thermoelectric responses to laser-induced heating. Such device-specific responses enable spatial and temporal information encoding, supporting parallel processing and reconfigurable architectures. By dynamically modulating laser activation patterns, the system achieves hierarchical computations, addressing tasks such as spiking neural networks [44–46], reservoir computing, and addressable multistate memory [47, 48] arrays. Furthermore, the pulsed thermoelectric outputs from the first layer can serve as inputs for a second layer, enabling sequential and hierarchical information processing. In this configuration, the second layer operates without additional biasing, relying solely on the output signals of the first layer. This layered design enhances energy efficiency while supporting adaptive computations, where each layer refines or transforms the information passed from the previous one. This hierarchical approach mirrors biological neural networks and opens pathways to modular, scalable architectures for advanced AI applications, including spatiotemporal processing, real-time decision-making, multistage logic operations, and high-precision analog computing.

II. A: DEVICE FEATURES AND LASER IRRADIATION SETUP

An array of spin-transfer torque nano-oscillators (STNOs) was fabricated, featuring magnetic tunnel junction (MTJ) nanopillars with cross-sectional geometries ranging from circular to elliptical shapes of varying radii (Fig. 1(b)). Each nanopillar was embedded within a SiO_2 dielectric layer and engineered with a multilayered structure optimized for performance, ensuring uniformity across all devices. The free layer comprised $\text{CoFe}_{40}\text{B}_{20}$ (2)/Ta (0.21)/ $\text{Ni}_{80}\text{Fe}_{20}$ (7)/Ta (10)/Ru (7), while a sacrificial layer of TiWN (15) and AlSiCu (100) facilitated the connection between the magnetic layers and the top contact. Magnetic sta-

bility was achieved by integrating a synthetic antiferromagnet (SAF) layer consisting of Ta (5)/Ru (5)/IrMn (6)/CoFe₃₀ (2)/Ru (0.7)/CoFe₄₀B₂₀ (2.6). The bottom contact was constructed as Ta (5)/CuN (50)/Ta (5)/CuN (50)/Ta (5)/Ru (5). All thicknesses are given in nanometers. To enhance optical accessibility, an indium tin oxide (ITO) top contact was employed [49–51].

To investigate the influence of laser-induced thermal gradients on STNO dynamics, we employed a modulated diode laser (638 nm wavelength, 1 kHz modulation frequency) focused to a 7 μm diameter spot. Calibrated laser powers of 30, 60, 90, 120, and 150 mW at the source corresponded to effective powers of 15, 28, 41, 54, and 67 mW incident on the sample surface, accounting for optical losses. The periodic laser illumination creates a temperature gradient across the nanopillar tunnel barrier, resulting in a pulsed thermoelectric voltage (V_{AC}). The system also enables the application of a bias current to achieve precise control over transport phenomena. The bias current generates a DC voltage (V_{DC}), while the laser-induced heating superimposes an AC voltage on this DC background. For open-circuit conditions ($I_{\text{bias}} = 0$), $V_{\text{DC}} = 0$. The AC and DC voltage components were subsequently separated and independently measured using dedicated electronic circuitry (Fig. 1). Notably, sweeping the magnetic field reveals hysteretic switching in both V_{AC} and V_{DC} , with distinct values observed for parallel (P) and antiparallel (AP) magnetization states. This tunable multistate behavior suggests potential applications in memory and logic devices.

III. EXPERIMENTAL RESULTS AND DISCUSSION

A. B: Thermoelectric Response of STNOs with Circular Nanopillars

The V_{AC} , representing the Seebeck voltage, originates from the thermal excitation of charge carriers driven by the temperature gradient established across the nanopillar tunnel barriers [52–55]. This thermoelectric response is intrinsically linked to the asymmetry of electronic states around the Fermi level within the ferromagnetic layers [40, 54, 56]. This asymmetry results in a difference in the density of states of spin-up and spin-down electrons at the Fermi level, leading to a spin-dependent Seebeck effect. The Seebeck voltage is highly sensitive to the magnetic configuration of the nanopillar, and by sweeping the DC magnetic field, it exhibits hysteretic switching behavior corresponding to transitions between

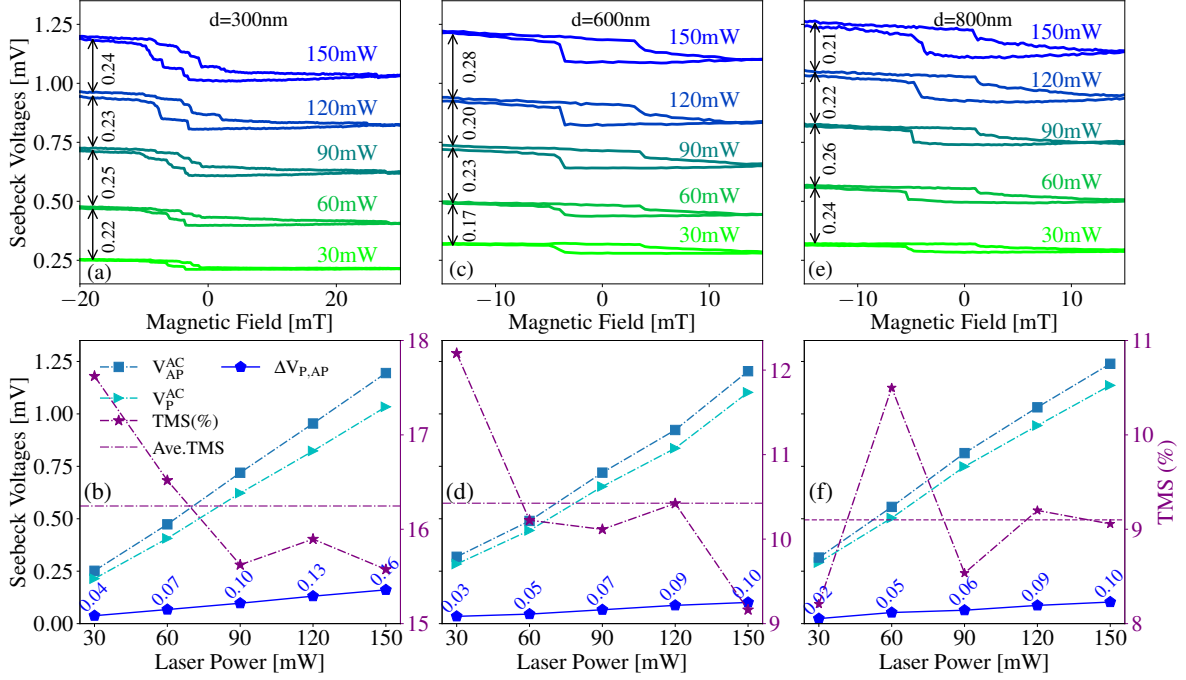


FIG. 2. Seebeck voltage as a function of magnetic field for varying laser powers in STNOs with nanopillar diameters of 300 nm ((a) and (b)), 600 nm ((c) and (d)), and 800 nm ((e) and (f)).

P and AP magnetization states. This pronounced sensitivity forms the basis of the tunnel magneto-Seebeck (TMS) effect, where the contrast in Seebeck voltages between P and AP states provides a reliable mechanism for device readout and spintronic logic operations.

First, we investigate the TMS effect under open-circuit conditions in STNOs with circular nanopillars. Systematic magnetic field sweeps were performed for each laser power, revealing distinct hysteresis loops characterized by P and AP states, with corresponding AC Seebeck voltages (V_P^{AC} and V_{AP}^{AC}). Notably, the magnetic field values at which the P and AP states occur in V_{AC} align with those observed in magnetoresistance measurements of biased STNO devices. The thermoelectric voltage (V_P^{AC} and V_{AP}^{AC}) is related to the Seebeck coefficient (S) and the applied temperature gradient (ΔT) as $V_{P/AP}^{AC} = S_{P/AP}\Delta T$ where S_P and S_{AP} are the Seebeck coefficients for the parallel and antiparallel magnetization states, respectively. Analogous to the tunnel magnetoresistance (TMR) ratio, we define the TMS effect ratio as:

$$\text{TMS} = \frac{S_P - S_{AP}}{\min(|S_P|, |S_{AP}|)} \equiv \frac{V_P - V_{AP}}{\min(|V_P|, |V_{AP}|)}. \quad (1)$$

As the $S_{p,ap}$, along with their corresponding voltages, can take negative values, division by the minimum absolute value ensures a meaningful ratio. Fig. 2(a), (c), and (e) present the

measured Seebeck voltage as a function of applied magnetic field for STNOs with 300 nm, 600 nm, and 800 nm nanopillars under varying laser powers. The extracted values of (V_P^{AC}) and (V_{AP}^{AC}), their difference ($\Delta V_{P,AP} = V_P^{AC} - V_{AP}^{AC}$) and the resulting TMS ratio are shown in Fig. 2(b), (d), and (f) as a function of laser power. Notably, devices with 300 nm nanopillars demonstrate a larger $\Delta V_{P,AP}$ and TMS ratios, likely attributed to steeper thermal gradients, improved homogeneity that reduces carrier scattering, and enhanced asymmetry in the electronic density of states at the nanoscale. Importantly, the millivolt-range Seebeck voltages are CMOS-compatible, eliminating biasing wires and enabling efficient integration for scalable computing systems. The linear dependence of V_P^{AC} , V_{AP}^{AC} and $\Delta V_{P,AP}$ on laser power, consistent with $V_{P/AP}^{AC} = S_{P/AP}\Delta T$, underscores the precise tunability of thermoelectric responses. This tunable output voltage offers significant potential for neuromorphic computing, where it can emulate synaptic weights, and for analog computing, where its continuous, linear behavior is ideal for approximating neuron activation functions and processing continuous variables. Additionally, the demonstrated sensitivity to temperature and magnetic fields highlights potential applications in high-resolution sensor technologies.

To extend the functionality of the TMS effect and investigate its potential for advanced applications, we introduce the Bias-Enhanced Tunnel Magneto-Seebeck (bTMS) effect [57, 58], which provides enhanced precision in controlling transport properties. Through the analysis of voltage variations using the Onsager transport equation [59, 60], the voltage difference between laser on and off states under conditions with and without laser-induced heating in the STNO can be expressed as:

$$\Delta V_{P,AP} = V_{on} - V_{off} = S_{P,AP}\Delta T + (R_{P,AP} - \Delta R_{P,AP})I - R_{P,AP}I, \quad (2)$$

where R is the resistance of the non-heated MTJ, and $R - \Delta R$ is the resistance when the STNO is heated. To quantify the on/off switching of the measured AC voltage induced by magnetization reversal, we defined a bTMS ratio as

$$\text{bTMS} = \frac{\Delta V_P - \Delta V_{AP}}{\min(|\Delta V_P|, |\Delta V_{AP}|)}. \quad (3)$$

The AC voltage as a function of the magnetic field for devices with nanopillar diameters of 300 nm ((a), (b)), 600 nm ((d), (e)), and 800 nm ((g), (h)) is presented in Fig. 3. Measurements were conducted under positive bias currents of 0.5 mA ((a), (d), (g)) and negative bias currents of -0.5 mA ((b), (e), (h)) for varying laser powers. These measurements

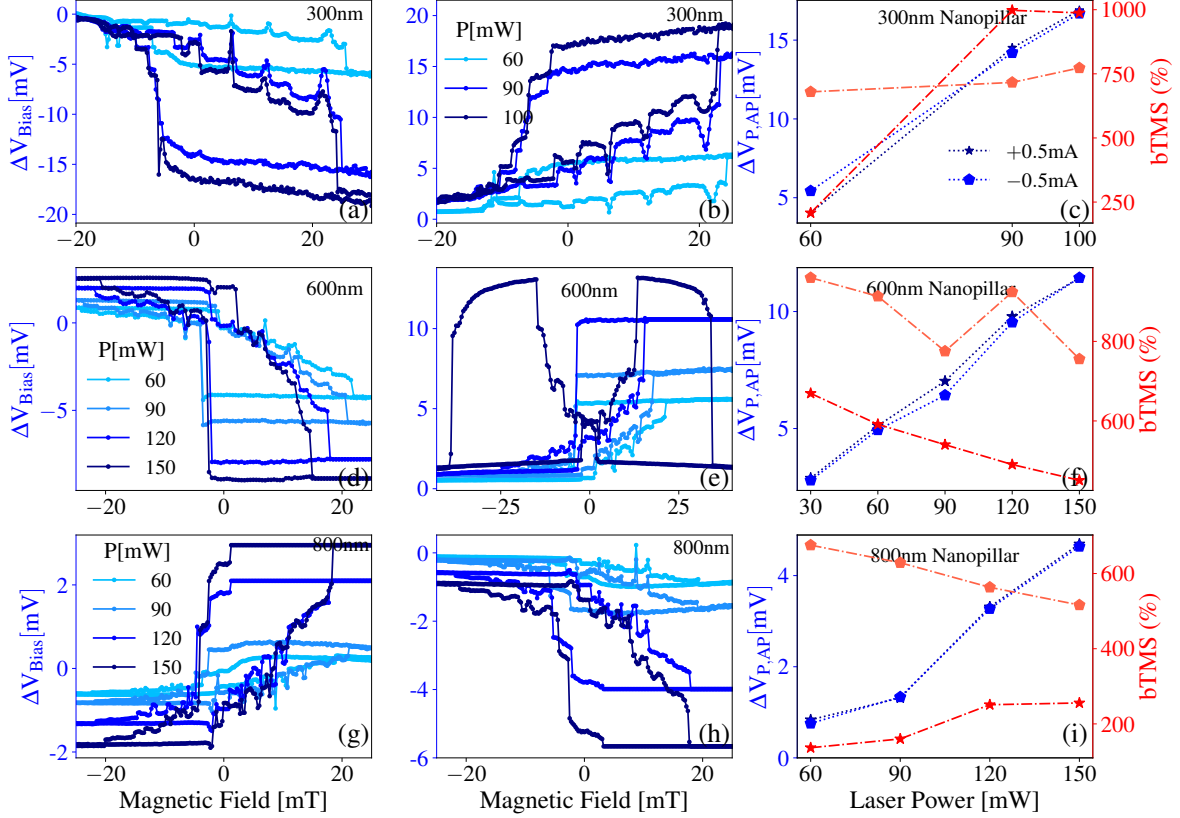


FIG. 3. The voltage ΔV_{bias} as a function of the magnetic field for various laser powers at a bias current of +0.5 mA (a, d, g), with corresponding measurements at a bias current of -0.5 mA (b, e, h). The resulting bTMS ratios and voltage differences between P and AP states (c, f, and i).

revealed a giant thermoelectric voltage with pronounced contrast between P and AP states, significantly enhancing the signal-to-noise ratio and readout precision.

As shown in SM [61], the tunneling magnetoresistance (TMR) curves of these devices exhibit discrete step-like features, which, depending on the device dimensions, can be attributed to different phenomena. For devices with smaller cross-sections ($d=300\text{nm}$), these steps are caused by Barkhausen jumps, arising from the motion of magnetic domains overcoming pinning sites [62, 63]. In contrast, for devices with larger diameters ($d=600, 800\text{nm}$), the free layer stabilizes a vortex magnetization state. This flux-closure configuration minimizes magnetostatic energy and becomes energetically favorable once the device dimensions exceed a critical threshold [64]. In such cases, the resistance steps are linked to jumps between local pinning sites of the vortex core, residing at the center of the vortex magnetization state, as detailed in [65]. Remarkably, under AC laser illumination, the thermovoltage out-

put exhibits sharp spikes precisely at the magnetic field values where the resistance steps occur. This correlation highlights the thermovoltage’s extreme sensitivity to abrupt magnetization changes, whether driven by domain wall motion or vortex-core dynamics. This nonlinear response provides insights into fundamental phenomena such as vortex and domain wall dynamics, pinning forces, and magnetization switching, while also suggesting potential applications in highly sensitive magnetic field sensors and unconventional computing architectures. The discrete thermovoltage jumps at specific magnetic fields present opportunities for multi-state synaptic devices, where intermediate magnetization/vortex states encode information with high fidelity. Additionally, the nonlinear magnetization dynamics act as a robust physical reservoir for reservoir computing [66], enabling the mapping of complex input signals—such as magnetic field variations or thermal gradients—into a high-dimensional feature space. The system’s ability to retain memory of past inputs through dynamic magnetization behavior supports demanding computational tasks, including chaotic time-series prediction and real-time classification, as demonstrated for similar spintronic systems [67]. While the present study does not address time-resolved dynamics, the sharp thermovoltage spikes highlight the system’s potential for high-resolution magnetic field sensing and advanced computational frameworks, warranting further investigation.

As shown in Fig. 3(e), the 600 nm STNO exhibits an unconventional double-switching behavior at a threshold bias current of $I = -0.5$ mA and laser power of $P = 150$ mW. This behavior is consistently observed across all devices when the bias current and laser power exceed specific threshold values. Results for the 600 nm and 800 nm devices are presented in Fig. 4, while the corresponding behavior for the 300 nm device is detailed in the SM [61]. The precise origin of this double-switching behavior remains an open question, potentially arising from nonlinear magnetization dynamics or instabilities in the fixed magnetic layer. At elevated laser powers and bias currents, the combined effects of thermal gradients and spin-transfer torque may push the system into a nonlinear regime [68–70], leading to complex switching phenomena characterized by multiple magnetization transitions. Alternatively, the extreme experimental conditions could destabilize the fixed layer, inducing precessional motion or partial magnetization reversal that affects the overall device response. These scenarios emphasize the need for further investigation, particularly time-resolved magnetization measurements, to fully understand the underlying mechanisms and their implications for spintronic applications. Such behavior could also have implications

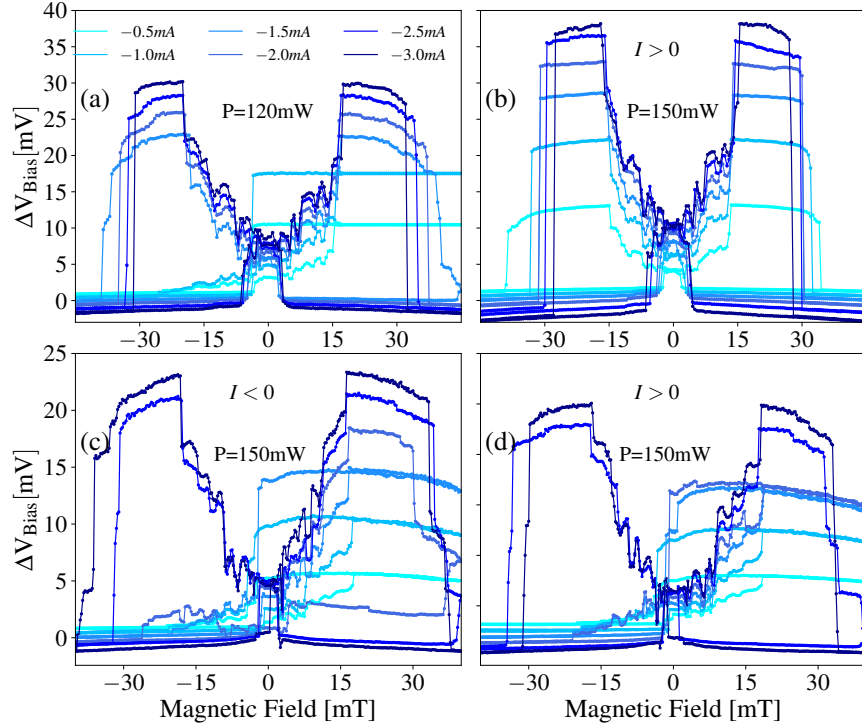


FIG. 4. The measured thermovoltage, ΔV_{bias} , as a function of the external magnetic field for a nanopillar with $d = 600$ nm (a and b) and $d = 800$ nm (c and d), at varying laser power and bias current.

for neuromorphic computing, where it may emulate synaptic responses for adaptive learning systems.

B. C: Thermoelectric Effects in STNOs with Elliptical Nanopillars

STNOs with elliptical cross-sections exhibit in-plane magnetic anisotropy, stabilizing two energetically favorable antiparallel magnetization states along the major axis, thus enabling binary encoding (0 and 1). TMS measurements for two STNOs with dimensions of $73 \times 276 \text{ nm}^2$ (eccentricity, $e=0.96$) and $200 \times 400 \text{ nm}^2$ ($e=0.87$) are presented in Fig. 5. The smaller elliptical nanopillar ($73 \times 276 \text{ nm}^2$) exhibits greater shape anisotropy and a stronger demagnetizing field, resulting in a higher energy barrier for magnetization switching. Consequently, a stronger external magnetic field is required to overcome this barrier, as evidenced by the increased switching field compared to the larger one (see Fig. 5). Increasing laser power reduces the switching field by lowering the energy barrier and decreasing the satura-

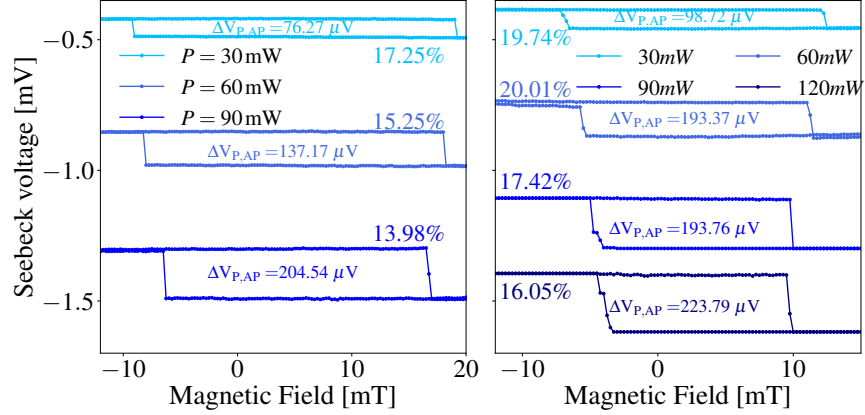


FIG. 5. Magnetic field and laser power dependence of the tunnel thermovoltage in STNOs with elliptical nanopillar: (a) $73 \times 276 \text{nm}^2$ and (b) $200 \times 400 \text{nm}^2$. Related TMS ratio values are presented adjacent to each curve.

tion magnetization, thereby weakening the demagnetizing field. Additionally, these elliptical STNOs, despite their smaller size relative to the circular 300 nm devices, exhibit a larger voltage difference ($\Delta V_{P,AP}$), indicating a higher contrast between the parallel (P) and antiparallel (AP) states.

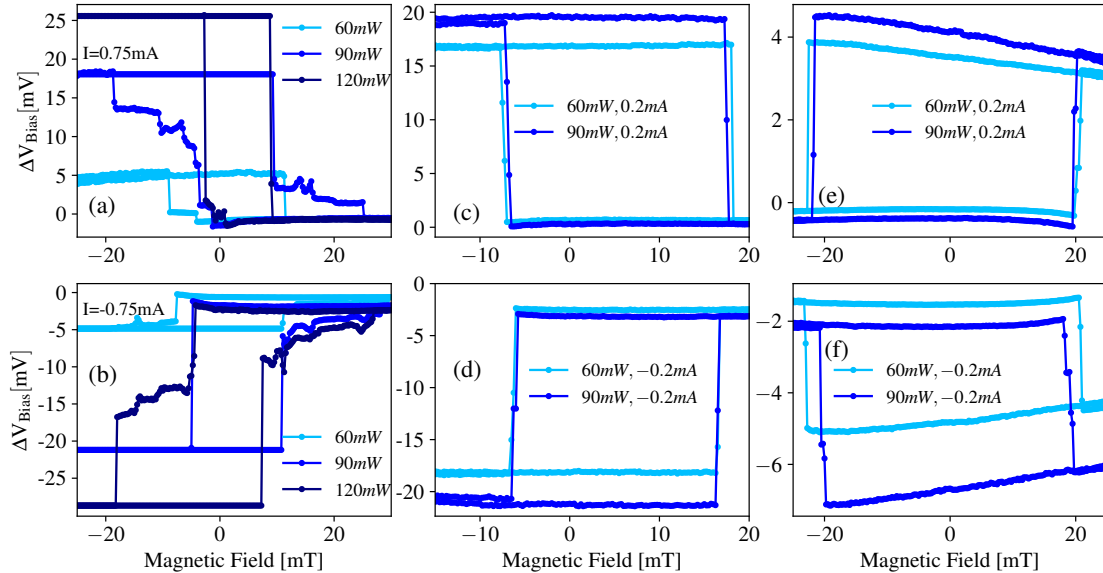


FIG. 6. ΔV_{bias} as a function of the magnetic field for varying laser powers and bias currents in STNOs with elliptical nanopillars: (a) and (b) $200 \times 400 \text{nm}^2$ ($e=0.87$), (c) and (d) $73 \times 276 \text{nm}^2$ ($e=0.96$), and (e) and (f) $137 \times 583 \text{nm}^2$ ($e=0.97$).

ΔV_{bias} as a function of the magnetic field for varying laser powers and bias currents is shown in Fig. 6 for elliptical STNOs with different eccentricities (e). The $200 \times 400\text{nm}^2$ STNO, with a smaller e , demonstrates lower magnetic field switching thresholds and higher thermovoltage output compared to devices with greater eccentricities. Interestingly, the measured ΔV_{bias} displays small jumps, reminiscent of features commonly associated with vortex states. This suggests that elliptical nanopillars with smaller eccentricities may support vortex formation under specific laser power, potentially influencing device performance and stability. Our results demonstrate that arrays of STNOs with identical layer configurations but diverse cross-sectional geometries and dimensions on a single chip can generate a wide range of responses, which is critical for advanced computing applications.

IV. CONCLUSION

In summary, we have fabricated and optimized an array of spin-transfer torque nanoscillators (STNOs) with both circular and elliptical cross-sections. A key aspect of this work is the implementation of a hybrid excitation scheme, enabling independent or simultaneous activation via AC laser illumination and DC bias current. Laser illumination alone induced substantial millivolt-range thermoelectric voltages via the tunnel magneto-Seebeck (TMS) effect, demonstrating CMOS compatibility. This breakthrough paves the way for simplified, energy-efficient neuromorphic chip architectures with reduced wiring complexity. When combined with a bias current, the bias-enhanced TMS (bTMS) effect was observed, characterized by giant thermovoltage outputs and novel two distinct phenomena: thermovoltage spikes and double-switching behavior. The thermovoltage spikes, corresponding to vortex state transitions, reveal exceptional sensitivity to magnetization changes and provide crucial insights into vortex core dynamics, including gyrotropic motion and pinning site jumps—fundamental aspects for STNO behavior. In contrast, the double-switching behavior likely originates from either instabilities in the fixed layer, leading to partial magnetization reversal, or highly nonlinear magnetization dynamics within the free layer.

Beyond their fundamental significance, the pulsed nature of the output voltage in both TMS and bTMS regimes resembles the spiking behavior of biological neurons, suggesting potential applications in systems inspired by neuromorphic computing. This behavior enables the integration of large arrays of nanopillars, each optically excited at distinct frequencies and

sharing a common electrical output, creating an efficient frequency-multiplexing scheme. By employing frequency-selective devices in subsequent processing layers, this approach could reduce hardware complexity and enhance scalability [71]. Furthermore, the combination of optical excitation and frequency-encoded spintronic signal processing offers opportunities for hybrid photonic-spintronic architectures, which may contribute to advancements in adaptive computing and signal processing. Future time-domain studies will be crucial to unravel the transient dynamics of pulsed thermovoltage and double-switching behavior, providing further insights into their underlying mechanisms and potential applications in neuromorphic systems, high-resolution sensing, and multistate memory storage. Leveraging their unique properties, hybrid laser-STNO systems hold great promise for bridging the gap between fundamental spintronic physics and next-generation computing technologies.

V. ACKNOWLEDGMENT

This project was supported by funding from the European Union’s Horizon 2020 research and innovation program under grant agreement No. 899559 (SpinAge). We thank J. Walowski, T. Ahlgrimm, L. Vollroth, and M. Kohlmann for their support with the experimental setup and technical discussions.

-
- [1] R. W. Keyes, *Science* **195**, 1230 (1977).
 - [2] R. Keyes, *Proceedings of the IEEE* **89**, 227 (2001).
 - [3] R. E. Bryant, K.-T. Cheng, A. B. Kahng, K. Keutzer, W. Maly, R. Newton, L. Pileggi, J. M. Rabaey, and A. Sangiovanni-Vincentelli, *Proc. IEEE* **89**, 341 (2001).
 - [4] V. Dunjko and H. J. Briegel, *Rep. Prog. Phys.* **81**, 074001 (2018).
 - [5] G. M. Mallow, A. Hornung, J. N. Barajas, S. S. Rudisill, H. S. An, and D. Samartzis, **6**, 93 (2022).
 - [6] O. Ayoade, P. Rivas, and J. Orduz, *Data* **7**, 28 (2022).
 - [7] T. S. Parvini, V. A. Bittencourt, and S. V. Kusminskiy, *Phys. Rev. Res.* **2**, 022027 (2020).
 - [8] T. S. Parvini, A.-L. E. Romling, S. Sharma, and S. V. Kusminskiy, *arXiv preprint arXiv:2409.10659* (2024), <https://arxiv.org/abs/2409.10659>.

- [9] M. Davies, [Nat. Mach. Intell](#) **1**, 386 (2019).
- [10] D. Marković, A. Mizrahi, D. Querlioz, and J. Grollier, [Nat. Rev. Phys](#) **2**, 499 (2020).
- [11] N. K. Upadhyay, H. Jiang, Z. Wang, S. Asapu, Q. Xia, and J. Joshua Yang, [Adv. Mater. Technol.](#) **4**, 1800589 (2019).
- [12] S. Kumar, X. Wang, J. P. Strachan, Y. Yang, and W. D. Lu, [Nat. Rev. Mater.](#) **7**, 575 (2022).
- [13] K. S. Mohamed, *Neuromorphic Computing and Beyond* (Springer, 2020).
- [14] A. Shrestha, H. Fang, Z. Mei, D. P. Rider, Q. Wu, and Q. Qiu, [IEEE Circuits and Systems Magazine](#) **22**, 6 (2022).
- [15] J. B. Aimone, P. Date, G. A. Fonseca-Guerra, K. E. Hamilton, K. Henke, B. Kay, G. T. Kenyon, S. R. Kulkarni, S. M. Mniszewski, M. Parsa, *et al.*, *Neuromorphic Computing and Engineering* **2**, 032003 (2022).
- [16] D. Marković and J. Grollier, [Appl. Phys. Lett.](#) **117** (2020), 10.1063/5.0020014.
- [17] S. H. Sung, T. J. Kim, H. Shin, T. H. Im, and K. J. Lee, [Nat. Commun.](#) **13**, 2811 (2022).
- [18] N. Du, X. Zhao, Z. Chen, B. Choubey, M. Di Ventra, I. Skorupa, D. Bürger, and H. Schmidt, *Frontiers in neuroscience* **15**, 660894 (2021).
- [19] H. Chen, H. Li, T. Ma, S. Han, and Q. Zhao, [Sci. Technol. Adv. Mater.](#) **24**, 2183712 (2023).
- [20] N. Zins, Y. Zhang, C. Yu, and H. An, “Neuromorphic computing: A path to artificial intelligence through emulating human brains,” in *Frontiers of Quality Electronic Design (QED): AI, IoT and Hardware Security*, edited by A. Iranmanesh (Springer International Publishing, Cham, 2023) pp. 259–296.
- [21] W. Huang, X. Xia, C. Zhu, P. Steichen, W. Quan, W. Mao, J. Yang, L. Chu, and X. Li, [Nano-Micro Lett.](#) **13**, 1 (2021).
- [22] J. Grollier, D. Querlioz, K. Camsari, K. Everschor-Sitte, S. Fukami, and M. D. Stiles, [Nat. Electron.](#) **3**, 360 (2020).
- [23] J. Torrejon, M. Riou, F. A. Araujo, S. Tsunegi, G. Khalsa, D. Querlioz, P. Bortolotti, V. Cros, K. Yakushiji, A. Fukushima, *et al.*, [Nature](#) **547**, 428 (2017).
- [24] J. Zhou and J. Chen, [Adv. Electron. Mater.](#) **7**, 2100465 (2021).
- [25] T. Sadat Parvini, E. Paz, T. Böhnert, A. Schulman, L. Benetti, F. Oberbauer, J. Walowski, F. Moradi, R. Ferreira, and M. Münzenberg, [J. Appl. Phys.](#) **133** (2023).
- [26] N. Jha, A. Pariyar, T. S. Parvini, C. Denker, P. K. Vardhanapu, G. Vijaykumar, A. Ahrens, T. Meyer, M. Seibt, N. Atodiresei, *et al.*, [ACS Appl. Electron. Mater.](#) **5**, 1471 (2023).

- [27] M. Riou, F. A. Araujo, J. Torrejon, S. Tsunegi, G. Khalsa, D. Querlioz, P. Bortolotti, V. Cros, K. Yakushiji, A. Fukushima, H. Kubota, S. Yuasa, M. D. Stiles, and J. Grollier, in *2017 IEEE International Electron Devices Meeting (IEDM)* (2017) pp. 36.3.1–36.3.4.
- [28] J. Liu, T. Xu, H. Feng, L. Zhao, J. Tang, L. Fang, and W. Jiang, *Adv. Funct. Mater.* **32**, 2107870 (2022).
- [29] S. Jiang, L. Yao, S. Wang, D. Wang, L. Liu, A. Kumar, A. A. Awad, A. Litvinenko, M. Ahlberg, R. Khymyn, *et al.*, *Appl. Phys. Rev.* **11** (2024), 10.1063/5.0221877.
- [30] D. Yu, J. Kang, J. Berakdar, and C. Jia, *NPG Asia Mater.* **12**, 36 (2020).
- [31] A. Sengupta and K. Roy, in *2015 International Joint Conference on Neural Networks (IJCNN)* (2015) pp. 1–7.
- [32] X. Zhang, W. Cai, M. Wang, B. Pan, K. Cao, M. Guo, T. Zhang, H. Cheng, S. Li, D. Zhu, *et al.*, *Adv. Sci.* **8**, 2004645 (2021).
- [33] A. Kurenkov, S. DuttaGupta, C. Zhang, S. Fukami, Y. Horio, and H. Ohno, *Adv. Mater.* **31**, 1900636 (2019).
- [34] A. F. Vincent, J. Larroque, N. Locatelli, N. B. Romdhane, O. Bichler, C. Gamrat, W. S. Zhao, J.-O. Klein, S. Galdin-Retailleau, and D. Querlioz, *IEEE transactions on biomedical circuits and systems* **9**, 166 (2015).
- [35] A. S. Jenkins, L. S. E. Alvarez, S. Memshawy, P. Bortolotti, V. Cros, P. P. Freitas, and R. Ferreira, *Commun. Phys.* **4**, 107 (2021).
- [36] Y. Imai, K. Nakajima, S. Tsunegi, and T. Taniguchi, *Sci. Rep.* **12**, 21651 (2022).
- [37] D. Suess, A. Bachleitner-Hofmann, A. Satz, H. Weitensfelder, C. Vogler, F. Bruckner, C. Abert, K. Prügl, J. Zimmer, C. Huber, *et al.*, *Nat. Electron.* **1**, 362 (2018).
- [38] M. Kammerer, M. Weigand, M. Curcic, M. Noske, M. Sproll, A. Vansteenkiste, B. Van Waeyenberge, H. Stoll, G. Woltersdorf, C. H. Back, *et al.*, *Nat. Commun.* **2**, 279 (2011).
- [39] J.-Y. Chen, L. He, J.-P. Wang, and M. Li, *Phys. Rev. Appl.* **7**, 021001 (2017).
- [40] A. Boehnke, U. Martens, C. Sterwerf, A. Niesen, T. Huebner, M. von der Ehe, M. Meinert, T. Kuschel, A. Thomas, C. Heiliger, *et al.*, *Nat. Commun.* **8**, 1626 (2017).
- [41] Y. Xu, W. Lin, S. Petit-Watelot, M. Hehn, H. Rinnert, Y. Lu, F. Montaigne, D. Lacour, S. Andrieu, and S. Mangin, *J. Appl. Phys.* **119** (2016), 10.1063/1.4939966.
- [42] H. Yang, X. Hu, S. Sievers, T. Boehnert, M. Tarequzzaman, J. Costa, R. Ferreira, M. Bieler, and H. Schumacher, *J. Appl. Phys.* **124** (2018), 10.1063/1.5049890.

- [43] W. Lin, M. Hehn, L. Chaput, B. Negulescu, S. Andrieu, F. Montaigne, and S. Mangin, [Nat. Commun.](#) **3**, 744 (2012).
- [44] S. Ghosh-Dastidar and H. Adeli, [Int. J. Neural Syst.](#) **19**, 295 (2009).
- [45] Y. Hu, L. Deng, Y. Wu, M. Yao, and G. Li, [IEEE Trans. Neural Netw. Learn. Syst.](#) (2024), [10.1109/TNNLS.2024.3355393](#).
- [46] S. Yang, J. Wang, B. Deng, C. Liu, H. Li, C. Fietkiewicz, and K. A. Loparo, [IEEE Trans. Cybern.](#) **49**, 2490 (2018).
- [47] P. Rzeszut, J. Checiński, I. Brzozowski, S. Zietek, W. Skowroński, and T. Stobiecki, [Sci. Rep.](#) **12**, 7178 (2022).
- [48] B. Shen, H. Sun, X. Hu, J. Sun, J. Jiang, Z. Zhang, and A. Jiang, [Adv. Funct. Mater.](#) , [2315954](#) (2024).
- [49] W. Jin Hu, Z. Wang, W. Yu, and T. Wu, [Nat. Commun](#) **7**, 10808 (2016).
- [50] R. A. Maniyara, C. Graham, B. Paulillo, Y. Bi, Y. Chen, G. Herranz, D. E. Baker, P. Mazumder, G. Konstantatos, and V. Pruneri, [Apl Materials](#) **9** (2021), [10.1063/5.0040864](#).
- [51] M. S. Farhan, E. Zalnezhad, A. R. Bushroa, and A. A. D. Sarhan, [International Journal of Precision Engineering and Manufacturing](#) **14**, 1465 (2013).
- [52] K.-I. Uchida, S. Takahashi, K. Harii, J. Ieda, W. Koshibae, K. Ando, S. Maekawa, and E. Saitoh, [Nature](#) **455**, 778 (2008).
- [53] M. Czerner, M. Bachmann, and C. Heiliger, [Phys. Rev. B](#) **83**, 132405 (2011).
- [54] M. Walter, J. Walowski, V. Zbarsky, M. Münzenberg, M. Schäfers, D. Ebke, G. Reiss, A. Thomas, P. Peretzki, M. Seibt, *et al.*, [Nat. Mater.](#) **10**, 742 (2011).
- [55] L. Gravier, S. Serrano-Guisan, F. Reuse, and J.-P. Ansermet, [Phys. Rev. B](#) **73**, 024419 (2006).
- [56] R. Schmidt, F. Wilken, T. S. Nunner, and P. W. Brouwer, [Phys. Rev. B](#) **98**, 134421 (2018).
- [57] A. Boehnke, M. Milnikel, M. von der Ehe, C. Franz, V. Zbarsky, M. Czerner, K. Rott, A. Thomas, C. Heiliger, G. Reiss, *et al.*, [Sci. Rep.](#) **5**, 8945 (2015).
- [58] T. Kuschel, M. Czerner, J. Walowski, A. Thomas, H. W. Schumacher, G. Reiss, C. Heiliger, and M. Münzenberg, [J. Phys. D: Appl. Phys.](#) **52**, 133001 (2019).
- [59] L. Onsager, [Phys. Rev.](#) **37**, 405 (1931).
- [60] L. Onsager, [Phys. Rev.](#) **38**, 2265 (1931).
- [61] T. S. Parvini, F. Oberbauer, T. J. Winkel, T. Böhnert, A. Schulman, L. Benetti, F. Moradi, R. Ferreira, and M. Münzenberg, [Supplemental Material at \[URL will be inserted by publisher\]](#)

- for [give brief description of material]..
- [62] M. Kuepferling, S. Zullino, A. Sola, B. Van de Wiele, G. Durin, M. Pasquale, K. Rott, G. Reiss, and G. Bertotti, *J. Appl. Phys.* **117** (2015), 10.1063/1.4908142.
 - [63] F. Bohn, G. Durin, M. A. Correa, N. R. Machado, R. D. Della Pace, C. Chesman, and R. L. Sommer, *Sci. Rep.* **8**, 11294 (2018).
 - [64] M.-W. Yoo, J. Lee, and S.-K. Kim, *Applied Physics Letters* **100** (2012), <https://doi.org/10.1063/1.4705690>.
 - [65] A. S. Jenkins, L. Martins, L. C. Benetti, A. Schulman, P. Anacleto, M. S. Claro, I. Caha, F. L. Deepak, E. Paz, and R. Ferreira, *Commun. Mater.* **5**, 7 (2024).
 - [66] M. Riou, J. Torrejon, F. Abreu Araujo, S. Tsunegi, G. Khalsa, D. Querlioz, P. Bortolotti, N. Leroux, D. Marković, V. Cros, *et al.*, *Reservoir Computing: Theory, Physical Implementations, and Applications*, 307 (2021).
 - [67] S. Shreya, A. Jenkins, Y. Rezaeiyan, R. Li, T. Böhnert, L. Benetti, R. Ferreira, F. Moradi, and H. Farkhani, *Sci. Rep.* **13**, 16722 (2023).
 - [68] Z. Zeng, G. Finocchio, and H. Jiang, *Nanoscale* **5**, 2219 (2013).
 - [69] M. Romera, E. Montebianco, F. Garcia-Sanchez, B. Delaët, L. D. Buda-Prejbeanu, and U. Ebels, *Appl. Phys. Lett.* **106** (2015), 10.1063/1.4921097.
 - [70] V. Uzunova and B. A. Ivanov, *Phys. Rev. B* **108**, 064423 (2023).
 - [71] N. Leroux, A. Mizrahi, D. Marković, D. Sanz-Hernández, J. Trastoy, P. Bortolotti, L. Martins, A. Jenkins, R. Ferreira, and J. Grollier, *Neuromorphic Computing and Engineering* **1**, 011001 (2021).